Demonstrations of the Efficacy of the BBP Validation Gauntlets for Building Response Analysis Applications

Stanford | ENGINEERING
Civil & Environmental Engineering

Kuanshi Zhong[1], Wen-Yi Yen[1], Ting Lin[2], Gregory Deierlein[1]

[1]Stanford University, [2]Marquette University

OPUS College of Engineering
MARQUETTE UNIVERSITY

1. Introduction and Previous Research on Broadband Platform (BBP) Validation

This poster presents an update on the comparative study between recorded (NGA-West) and simulated ground motions (BBP, Fig. 1) to evaluate the feasibility of using the latter in engineering practices (the structural nonlinear time history analysis and the collapse assessment).

This study is part of a larger project, organized through the Ground Motion Simulation Validation (GMSV), to demonstrate the capabilities and limitations of the BBP to develop synthetic seismographs for engineering applications and the efficacy of the BBP validation gauntlets to screen the BBP seismographs. Supporting this study are related effort to validate BBP motions for past earthquakes, develop and process BBP motions for scenario-based earthquake realizations, and to demonstrate correlation between results of validation gauntlets and building response comparisons.

This study also follows and expands the previous research efforts on the validation of BBP for tall building risk assessment by Bijelić, Lin and Deierlein (2014-2017).

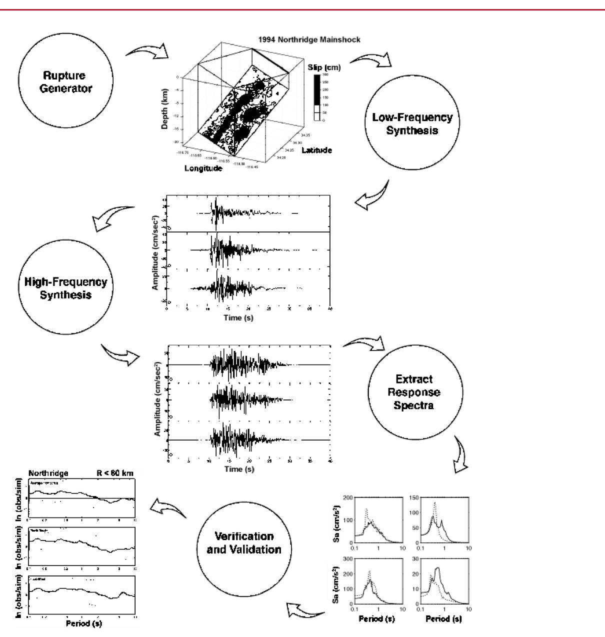

Figure 1. Broadband Platform (BBP) (SCECpedia)

2. Site, Seismic Hazard, and Ground Motion Database

Three sites along the west coast are selected in this study in San Francisco downtown (SFDT), Los Angeles downtown (LADT), and San Bernardino (SB). The SFDT site (8029-RIN, -122.4 W, 37.8 N, Vs30 = 873 m/s) is dominated by two major sources (North San Andreas ~90% and Hayward ~10%). The LADT (-118.3 W, 34.1 N, Vs30 = 390 m/s) and SB (S688, -117.3 W, 34.1 N, Vs30 = 280 m/s) sites have more complex multi-source features, with multiple faults contributing to the hazard. For this demonstration BBP motions are developed for two sources for LADT and SB.

Two ground-motion databases are used in this study: (1) NGA-West and (2) BBP that is recently released by SCEC. The promise of BBP database is not only that it has the simulated motions occurred and recorded at the sites of interest, but also that more motions from more severe events with large magnitudes and near-fault features are available for a potentially better representation of the local seismic hazard.

The BBP (v17.3.0) motions developed for this study are from the following: SFDT - 1152 records from M8.0 North San Andreas and 576 records from M7.0 Hayward/Rogers Creek; LADT - 704 records from M6.6 Elysian Park and 352 records from M7.9 South San Andreas; SB 1408 records from M7.8 San Jacinto and 352 records from M7.9 South San Andreas.

3. Ground Motion Selection and Comparison between Selected NGA and BBP Motions

The generalized conditional intensity measure (GCIM) approach (Bradley, 2010) is used to compute site- and source-specific targets for conditional spectra (CS) and conditional significant durations. 100 ground motions are selected and scaled at each of the three intensity levels (10% in 50 years Design-Based Earthquake, 2% in 50 years Maximum Considered Earthquake, and 2% in 200 years extreme earthquake) and scaled to the GCIM targets, by adapting a ground-motion selection algorithm (Jayaram et al., 2011) to include both spectral and duration metrics in the selection criteria.

We used the Campbell-Bozorgnia (2008) to determine target pseudo spectra and Afshari-Stewart (2016) to determine target duration metrics. Inter-period spectral acceleration correlation (Baker, 2010) and spectral acceleration-significant duration correlation (Bradley, 2011) are applied in computing target conditional spectra.

Both ground motion databases provide good selection results for San Francisco site and the South San Andreas events, but a discrepancy is observed in selecting BBP ground motions to represent the hazard from Elysian Park event (Fig. 2). Selected NGA and BBP motions for the South San Andreas and Elysian Park events are summarized in Tables 1-3, where the number of ground motions in each set is based on hazard deaggregation. Note that the required scaling factors are much less for the BBP motions as compared to the NGA motions, which is a key incentive for using the BBP motions.

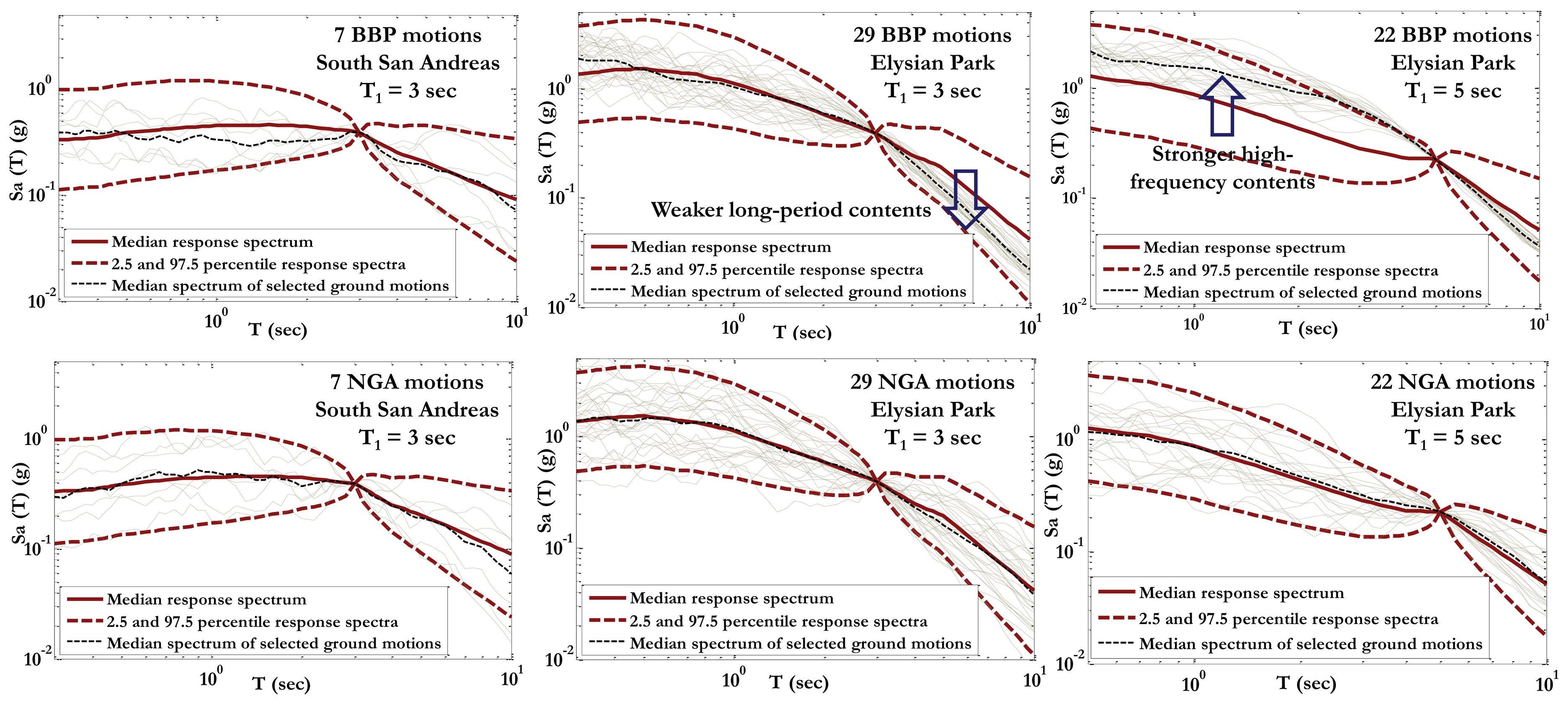

Figure 2. Comparison of source-specific ground-motion selection results at LADT (2% in 200 years).

Table 1. Selected ground motions for South San Andreas (T_1 = 3.0 sec, 2% in 200 years).

BBP		NGA	
Record name	Scaling factor	Record name	Scaling factor
T2.gp-safr01-01r.1004.la001.EW	0.86	RSN2486_CHICHI.03_CHY066N	8.08
T2.gp-safr01-01r.1006.sb001.NS	0.69	RSN1629_STELIAS_059V3279	2.29
T2.gp-safr01-01r.1002.sb006.EW	4.08	RSN1610_DUZCE_KUT090	4.00
T2.gp-safr01-01r.1004.la008.EW	0.62	RSN1472_CHICHI_TCU017-E	4.33
T2.gp-safr01-01r.1006.la008.EW	0.92	RSN1562_CHICHI_TTN006-E	9.94
T2.gp-safr01-01r.1008.sb009.EW	6.61	RSN1152_KOCAELI_BRV090	37.03
T2.gp-safr01-01r.1007.sb009.NS	3.75	RSN1174_KOCAELI_TOS090	19.63

Table 2. Selected ground motions for Elysian Park (T_1 = 5.0 sec, 2% in 200 years).

BBP		NGA	
Record name	Scaling factor	Record name	Scaling factor
T2.gp-epfr02-16r.10000011.la004.NS	1.83	RSN1452_CHICHI_TAP086-E	11.10
T2.gp-epfr02-16r.10000007.la002.NS	2.46	RSN1148_KOCAELI_ARE090	2.13
T2.gp-epfr02-16r.10000007.la004.NS	2.09	RSN1492_CHICHI_TCU052-E	0.58
T2.gp-epfr02-16r.10000009.la002.NS	1.70	RSN2466_CHICHI.03_CHY035N'	16.81
T2.gp-epfr02-16r.10000011.la007.NS	2.16	RSN1114_KOBE_PRI090	2.24
T2.gp-epfr02-16r.10000007.la005.NS	2.09	RSN183_IMPVALL.H_H-E08230	1.79
T2.gp-epfr02-16r.10000004.la005.NS	1.96	RSN181_IMPVALL.H_H-E06230	1.04
T2.gp-epfr02-16r.10000012.la004.NS	2.22	RSN1158_KOCAELI_DZC270	2.91
T2.gp-epfr02-16r.10000006.la004.NS	1.77	RSN1824_HECTOR_DRW016	11.61
T2.gp-epfr02-16r.10000009.la005.NS	1.70	RSN179_IMPVALL.H_H-E04230	1.16
T2.gp-epfr02-16r.10000006.la005.NS	1.88	RSN173_IMPVALL.H_H-E10050	2.38
T2.gp-epfr02-16r.10000010.la001.NS	2.85	RSN1505_CHICHI_TCU068-E	0.62
T2.gp-epfr02-16r.10000008.la002.NS	2.04	RSN182_IMPVALL.H_H-E07230	1.35
T2.gp-epfr02-16r.10000012.la005.NS	2.14	RSN749_LOMAP_UCS135	15.87
T2.gp-epfr02-16r.10000004.la002.NS	2.14	RSN1161_KOCAELI_GBZ000	1.95
T2.gp-epfr02-16r.10000008.la004.NS	1.82	RSN1605_DUZCE_DZC270	0.89
T2.gp-epfr02-16r.10000015.la004.NS	1.75	RSN2461_CHICHI.03_CHY028N	6.63
T2.gp-epfr02-16r.10000006.la002.NS	1.94	RSN1182_CHICHI_CHY006-W	2.53
T2.gp-epfr02-16r.10000001.la005.NS	2.11	RSN798_LOMAP_TLH090	16.69
T2.gp-epfr02-16r.10000004.la004.EW	1.91	RSN900_LANDERS_YER270	2.51
T2.gp-epfr02-16r.10000008.la005.NS	1.88	RSN2114_DENALI_PS10-047	1.38
T2.gp-epfr02-16r.10000010.la005.NS	1.98	RSN1162_KOCAELI_GYN090	9.08

Table 3. Selected ground motions for Elysian Park (T_1 = 3.0 sec, 2% in 200 years).

BBP		NGA	
Record name	Scaling factor	Record name	Scaling factor
T2.gp-epfr02-16r.10000014.la005.NS	1.17	RSN2751_CHICHI.04_CHY100N	6.68
T2.gp-epfr01-16r.10000004.la004.NS	3.17	RSN179_IMPVALL.H_H-E04140	4.14
T2.gp-epfr01-16r.10000004.la011.NS	3.90	RSN1114_KOBE_PRI000	1.22
T2.gp-epfr02-16r.10000007.la005.NS	1.34	RSN2490_CHICHI.03_CHY074E	17.14
T2.gp-epfr02-16r.10000002.la010.NS	1.58	RSN1158_KOCAELI_DZC270	3.80
T2.gp-epfr02-16r.10000002.la003.NS	1.73	RSN185_IMPVALL.H_H-HVP225	2.29
T2.gp-epfr01-16r.10000003.la008.EW	2.42	RSN821_ERZINCAN_ERZ-EW	1.80
T2.gp-epfr02-16r.10000007.la002.NS	1.52	RSN775_LOMAP_SGI360	20.55
T2.gp-epfr02-16r.10000003.la004.NS	2.22	RSN2457_CHICHI.03_CHY024N	7.96
T2.gp-epfr02-16r.10000008.la002.NS	1.27	RSN1114_KOBE_PRI090	2.24
T2.gp-epfr01-16r.10000003.la002.NS	2.80	RSN507_SMART1.40_40M01NS	9.09
T2.gp-epfr02-16r.10000004.la004.EW	1.13	RSN777_LOMAP_HCH090	2.89
T2.gp-epfr02-16r.10000002.la002.EW	1.59	RSN2655_CHICHI.03_TCU122E	2.51
T2.gp-epfr02-16r.10000009.la004.NS	1.09	RSN803_LOMAP_WVC270	2.54
T2.gp-epfr01-16r.10000003.la009.NS	3.25	RSN982_NORTHR_JEN022	0.98
T2.gp-epfr02-16r.10000002.la007.NS	2.08	RSN3548_LOMAP_LEX000	2.22
T2.gp-epfr01-16r.10000006.la002.NS	3.65	RSN2465_CHICHI.03_CHY034N	8.40
T2.gp-epfr02-16r.10000004.la006.NS	1.98	RSN748_LOMAP_BES345	5.73
T2.gp-epfr02-16r.10000011.la004.NS	1.18	RSN2712_CHICHI.04_CHY042N	18.69
T2.gp-epfr02-16r.10000011.la007.NS	1.00	RSN2078_NENANA_K218090	31.91
T2.gp-epfr02-16r.10000007.la004.NS	1.34	RSN1505_CHICHI_TCU068-E	0.75
T2.gp-epfr02-16r.10000001.la007.EW	1.60	RSN1272_CHICHI_HWA023-N	12.50
T2.gp-epfr02-16r.10000011.la002.NS	0.98	RSN527_PALMSPR_MVH135	2.91
T2.gp-epfr02-16r.10000012.la004.NS	1.15	RSN795_LOMAP_PHT270	9.24
T2.gp-epfr02-16r.10000008.la003.NS	1.93	RSN795_LOMAP_PHT360	18.34
T2.gp-epfr02-16r.10000009.la005.NS	1.24	RSN2114_DENALI_PS10-047	0.99
T2.gp-epfr02-16r.10000001.la004.NS	1.36	RSN2496_CHICHI.03_CHY081E	9.72
T2.gp-epfr02-16r.10000015.la004.NS	0.97	RSN778_LOMAP_HDA255	2.98
T2.gp-epfr01-16r.10000003.la005.NS	3.47	RSN187_IMPVALL.H_H-PTS225	6.11

Note: Ground motions are selected to best match (1) target conditional spectrum and (2) target duration (Ds_{5-75}). Although not been shown in this poster, the median Ds_{5-75} of selected BBP and NGA motions are about 2 and 4 seconds respectively; while the target median Ds_{5-75} is 4.0 second ~ 4.5 second for Elysian Park source (T_1 = 3.0 sec and 5.0 sec, 2% in 200 years).

Shown in Fig. 3 are comparisons of the characteristics for the ground motions selected for the Elysian Park and South San Andreas events. SaRatio is a scalar that reflects the normalized spectral shape, where larger ratios tend to be more damaging to the structures.

Elysian Park:

- The median SaRatio of selected BBP records is higher than the NGA records.
- Selected BBP motions have less dispersion in Ds_{5-75}.

South San Andreas:

- Similar median SaRatios, but BBP motions have less dispersion
- Similar median Ds_{5-75}, and no significant bias in dispersions between the two motion sets.

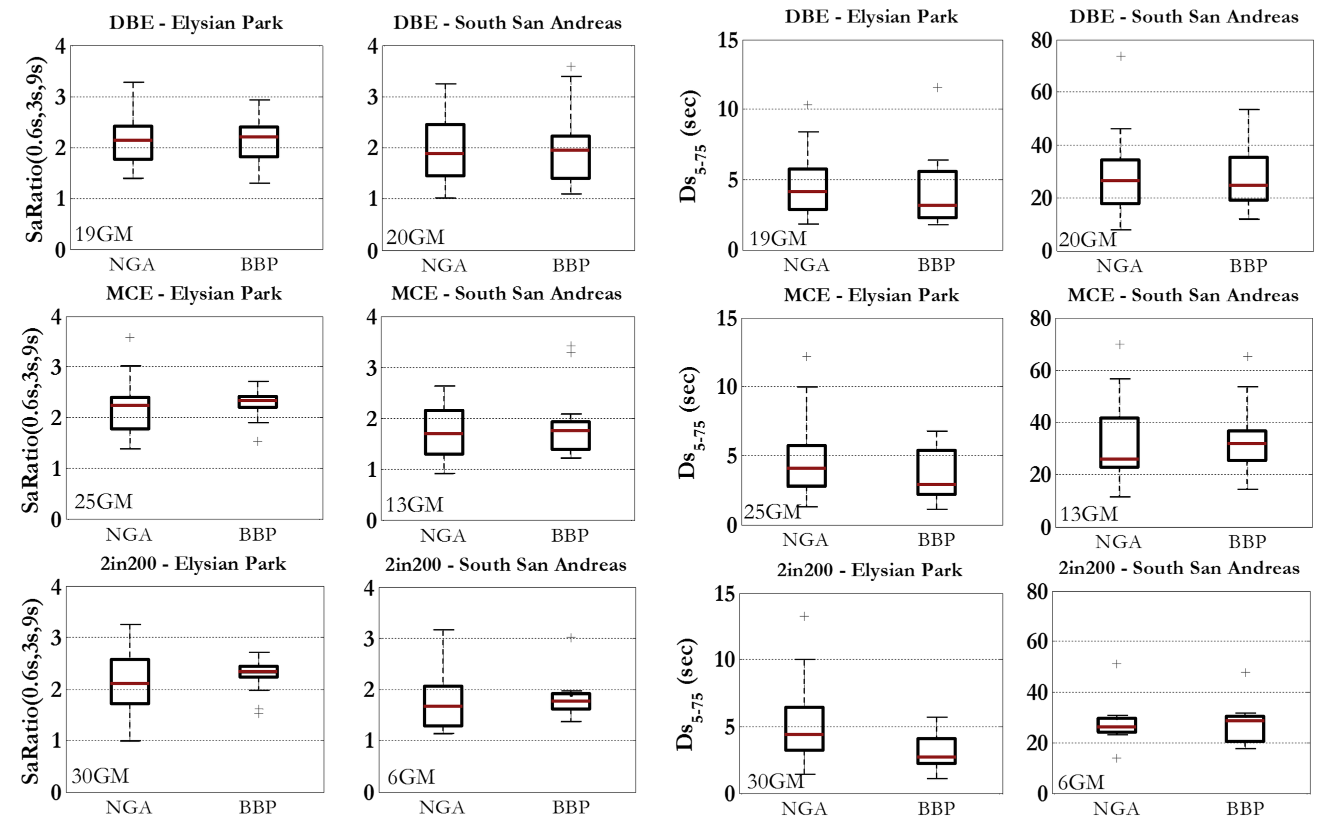

Figure 3. Comparison of selected ground motion characteristics: SaRatio and Ds_{5-75} (LADT, T_1 = 3.0 sec)

4. Nonlinear Time History Structural Analysis and Collapse Assessment

The archetype buildings analyzed include: (1) a 20-story reinforced concrete special moment frame (RCSMF) designed to California seismic hazard, and (2) a 43-story reinforced concrete wall structure (RCW) modified from the core-wall building in PEER TBI case studies (Moehle et al., 2011). The RCSMF is modeled by concentrated hinge beam-column elements with joint panel zones. The gravity system is considered as a series of leaning columns attached to the lateral frame. Illustrative results of the multi-stripe analysis (MSA) for the RCSMF for the SFDT and LADT sites are summarized in Fig. 4 and Table 4.

Comparing structural responses under BBP to NGA motions, less than 5% differences can be found in the median maximum story drift ratio (SDR_{max}) and the median peak floor acceleration (PFA) at DBE and MCE intensity levels. Larger differences, up to 15%, occur at 2%-in-200-yrs intensity level, which is mainly due to in part by the different number of observed collapses at this intensity.

The estimated median collapse intensities (S_{CT}) by two ground-motion sets also have less than 10% differences. The resulting mean annual frequency of collapse (λ_{col}) under BBP motions can deviate about 15% from the λ_{col} under NGA motions. The differences are mainly attributed to differences in how well the selected ground motions fit the target conditional spectra (T_1 = 3 sec., Fig.3)

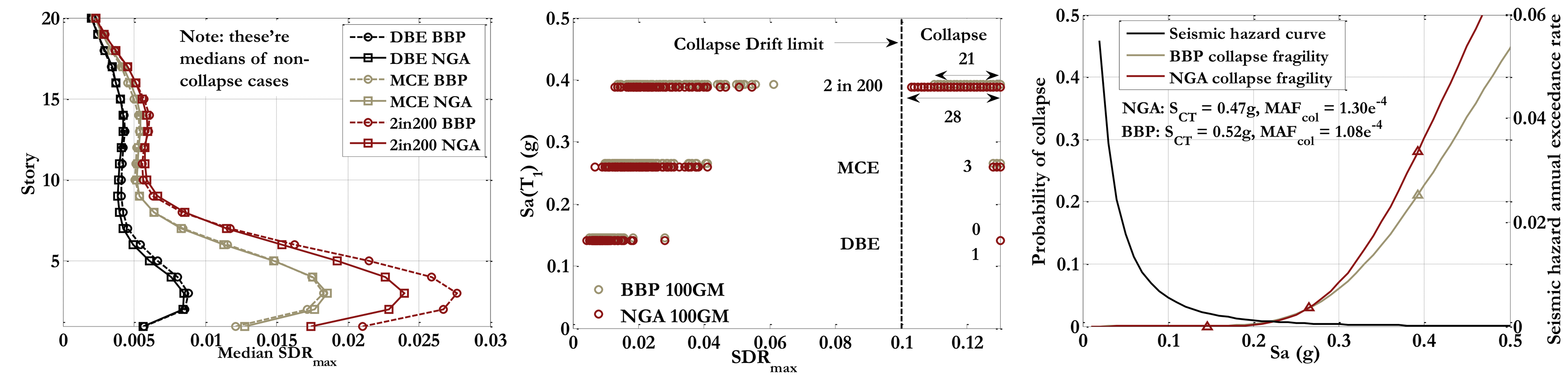

Figure 4. Comparison of maximum story drifts (SDR_{max}) and collapse probabilities of the 20-story RC frame subject to NGA and BBP motions at the LADT site.

Table 4. Summary of estimated structural responses and collapse risks.

Site	GM set	m (SDR_{max} | NC) (%)		m (PFA | NC) (g)		S_{CT} (g)		λ_{col} (x10^{-4})	
		NGA	BBP	NGA	BBP	NGA	BBP	NGA	BBP
SFDT	DBE	0.50	0.50	0.30	0.29	0.45	0.42	5.63	6.37
	MCE	1.27	1.24	0.38	0.36				
	2in200	2.04	1.89	0.44	0.40				
LADT	DBE	0.88	0.85	0.36	0.35	0.47	0.52	1.30	1.08
	MCE	1.86	1.83	0.48	0.50				
	2in200	2.40*	2.75	0.55*	0.65				

5. Collapse Risk Deaggregation

As shown in Figure 4, the main difference between two sets of results at LADT (2% in 200 years) is that the selected 100 NGA motions result in 7 more collapses than selected BBP counterparts do. To understand the underlying reason for this disagreement, collapse risk deaggregation is applied at that intensity level. Figure 5 shows the deaggregation results of (1) Elysian Park and (2) South San Andreas.

In lieu of the difference from South San Andreas results, it is observed that 8 collapses in the NGA set are out of 29 motions from Elysian-Park subset, while no collapse has been seen under BBP Elysian-Park motions. This is consistent with the ground motion characteristics shown in Figure 3. Comparing to selected NGA records, the median SaRatio of selected BBP Elysian-Park records is roughly 15% higher. The larger the SaRatio, the less damaging the ground motion (scaled to the same Sa (T_1)).

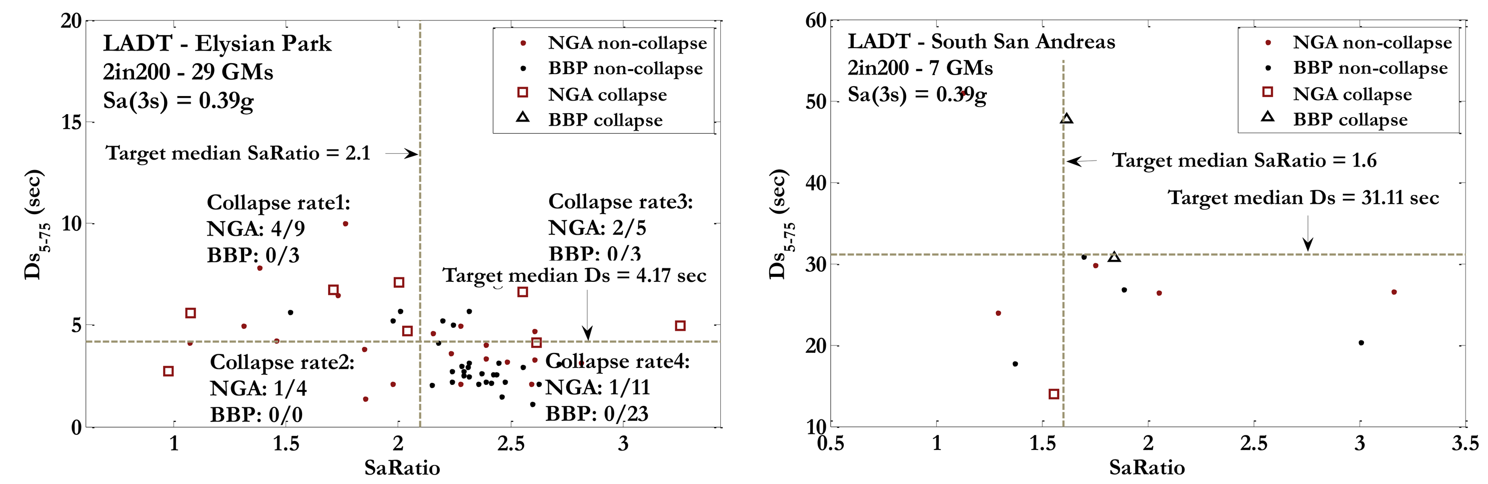

Figure 5. Collapse risk deaggreagation by sources (LADT, 2% in 200 years).

6. Summary

- BBP can serve as an alternative seismic input source in two presented case, where by simulating large events, less scaling is required to match BBP motions to high intensity targets.
- Bijelic et al (2017) and others have demonstrated that structural response and collapse are sensitive to differences in (1) Sa (T_1), (2) the spectral shape (SaRatio), (3) high-frequency contents, and (4) the duration metric (Ds_{5-75}). Differences in calculated building response observed in this study are mainly attributed to quality of fit of SaRatio's to the CS targets.

Acknowledgements

This research is supported by the Southern California Earthquake Center (SCEC project #16110) and the Blume Center for Earthquake Engineering. The authors gratefully acknowledge researchers associated with SCEC for developing and advancing ground motion simulations. In particular, the authors thank Nenad Bijelic, Reagan Chandramohan, Nico Luco, Robert Graves, Phil Maechling, Christine Goulet, Fabio Silva, Farzin Zareian, and Sanaz Rezaeian for their support and help. Great appreciations to PEER for providing the NGA database and Stanford/Blume Center for use of the Sherlock computing cluster at Stanford University.